2024 IEEE/RSJ International Conference on Intelligent Robots and Systems (IROS)
October 14-18, 2024. Abu Dhabi, UAE

Foot Arch Stiffness-Based Dynamic Plantar Support Control of Human Walking Gait with Active Pneumatic Insoles

Chenhao Liu, Jingang Yi, Long He, Yijun Zhang, Xiufeng Zhang and Tao Liu

Abstract— **The human foot arch plays a significant role in bearing weight, keeping balance, and walking efficiently. In this study, we present a pneumatic arch support insole (PASI) and a foot arch stiffness-based dynamic plantar support control to reduce the metabolic cost of walking. We first obtain the foot arch quasi-stiffness estimation over the gait phase by conducting multiple subject experiments. The design and modeling of the PASI and foot-insole interactions are then discussed. A model predictive control scheme is presented to dynamically regulate the foot arch stiffness over the gait phase by using the active PASI. We validate the system experimentally and conduct multi-subject walking tests. The results show that dynamic plantar support control of the foot arch stiffness reduces the metabolic cost by 7.99% compared to regular walking. In contrast, passive support without dynamic regulation increases the metabolic cost by 6.60%. The new pneumatic insoles and dynamic support method demonstrate promising potential for everyday and medical applications.**

I. Introduction

The human foot has a complex biomechanism that contains numerous bones, joints, muscles, ligaments, etc. Among them, the foot arch plays a vital role in bearing the weight of the human body, absorbing the ground impact [1], distributing the pressure on the sole [2], and maintaining balance [3]. In the ordinary course of human gait, sustained overloading, such as prolonged periods of standing, walking, or sports, can lead to fatigue and flattening of the foot arch and result in foot injuries and gait disorders (e.g., flat feet) [4]. To prevent excessive lowering of the foot arch and mitigate the associated risks of injury, many intervention and assistive devices were developed to support the foot arch, for example, foot orthoses [5], [6], orthopedic insoles [7]–[9], and flexible airbags [10]. The traditional orthopedic insole can ensure the standard height of the wearer's foot arch by adding rigid protrusions under the arch. Such rigid, passive support does not account for changes in foot arch stiffness and even restricts the degrees of freedom of the human foot, increasing the energy cost of running [11]. Moreover, prolonged use of those passive orthoses may lead to disuse atrophy of muscles [12]. Furthermore, the structure of the human foot arch changes with the aging process, resulting in the high long-term costs associated with custom orthopedic insoles. In [10], an inflatable airbag was used to achieve flexible foot arch support, but the air pressure of the airbag remained constant.

The shortcoming with traditional insoles lies in providing sufficient support but unable to adapt to the morphological changes occurring in the foot arch. Indeed, achieving a balance between these two objectives is intricate due to the passive nature of the arch. Pneumatic soft actuators (PSAs) are attractive for this challenge due to their inherent compliance for human-machine interaction (HMI) [13]. It is still essential to design an adaptive control strategy that dynamically adjusts plantar support based on the changing foot arch stiffness at different gait phases. While studies of electric motor-tendon wearable systems prioritize physical HMI and force tracking [14], PSAs still function at a low-level control such as pressure or position tracking due to their nonlinearity [15] and difficulty in theoretical modeling and HMI modeling. The development of analytical models for PSAs and the HMI models to achieve high-level control based on human motion's auxiliary needs or intentions remain open challenges [16]. Ker et al. [17] characterized the longitudinal arch of the foot as an elastic storage-return mechanism. This phenomenon occurs as the arch undergoes compression and recoil throughout the stance phase [17], [18]. Understanding the dynamically varying foot arch stiffness during the stance phase is crucial for designing and controlling foot orthoses, insoles, and other intelligent support devices for the lower limb.

This study presents a bio-inspired pneumatic arch support insole (PASI) and a foot arch stiffness-based dynamic plantar support control with PASI. The varying foot arch quasi-stiffness during the stance phase is defined and estimated through barefoot walking experiments. The overall design of the PASI and plantar support control strategy is then presented. Subsequently, a theoretical model for the PASI actuator is established, followed by a physical foot-insole interaction model. A model predictive control (MPC) scheme is proposed to optimize the gait-adaptive force-deformation trade-off and support control. We conduct extensive experiments to validate and demonstrate the PASI system and the MPC-based plantar support control by multiple subject

This work was supported in part by the NSFC Grant No. U1913601, No. 52175033 and No. U21A20120.

Chenhao Liu and Tao Liu are with the State Key Laboratory of Fluid Power and Mechatronic Systems, School of Mechanical Engineering, Zhejiang University, Hangzhou, Zhejiang 310027 China. liuchenhao@zju.edu.cn; liutao@zju.edu.cn.

Jingang Yi is with the Department of Mechanical and Aerospace Engineering, Rutgers University, Piscataway, NJ 08854 USA. jgyi@rutgers.edu.

Long He is with the Zhiyuan Research Institute, Hangzhou, Zhejiang 310024 China. helong_zyy@163.com.

Yijun Zhang is with the Department of Orthopedics, The First Affiliated Hospital, Zhejiang University School of Medicine, Hangzhou, Zhejiang 310003 China. zhangyijun87@zju.edu.cn.

Xiufeng Zhang is with the Key Laboratory of Rehabilitation Technical Aids Technology and System of the Ministry of Civil Affairs, National Research Center for Rehabilitation Technical Aids, Beijing 100176, China. zhangxiufeng@mca.gov.cn.

experiments. The results confirm that providing additional support for the foot arch with the new PASI device can effectively reduce walking energy expenditure. The new dynamic foot arch support system can be used not only in medical applications for preventing arch collapse and treating flat feet but also for assisting in everyday outdoor activities and maintaining balance.

The contribution of this study lies in the integrated novel control strategy and a soft PASI device capable of dynamically adjusting active assistance to accommodate the varying stiffness of the foot arch during walking gait. This dynamic assistance method mitigates uncomfortable interference on foot movement imposed by the soft actuator, addressing the shortcomings of traditional supportive insoles. Compliance with the inherent energy-saving mechanism of the foot arch, the new control design reduces energy consumption during walking, enabling wearable applications for foot assistance.

II. Foot Arch Quasi-Stiffness and Estimation

A. Foot Arch Quasi-Stiffness

Fig. 1(a) illustrates the foot anatomical structure and Fig. 1(b) shows the work and energy cyclic profile during gait phase [18]. The foot arch absorbs energy from the ground impact when compressed and then returns energy for propulsion when recoiled, with the dynamic quasi-stiffness of the foot arch changing constantly.

In this study, the definition of foot arch quasi-stiffness is adopted from [19]. Quasi-stiffness is defined for a cadaveric foot as the force applied vertically downward on the arch divided by its displacement. Measuring the stiffness variation of the foot arch in *vivo* is however practically impossible because the load on the foot arch cannot be directly measured. According to the basic minimal biped walking model [20], the ground reaction force (GRF) F_{GR} is considered equal to the body's weight on the foot, denoted by F_{BW}. Consequently, similar to [19], we define the instantaneous stiffness of the foot arch as the ratio of the changes of load applied to the foot and the foot arch height, that is,

$$K = \frac{\Delta F_{GR}}{\Delta h} \tag{1}$$

where K represents the foot arch quasi-stiffness, ΔF_{GR} and Δh are the changes of the applied load and foot arch height, respectively.

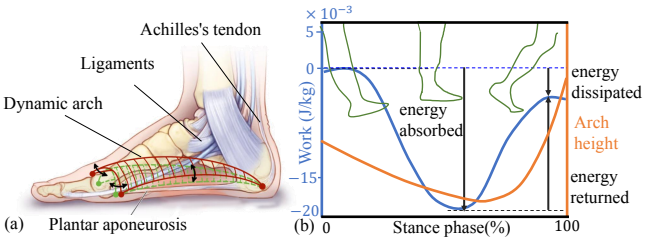

Fig. 1. (a) The shape of the foot and the dynamic arch. (b) Energetic of the foot arch, including an example of variation of foot arch height and work done by foot arch during stance phase [18].

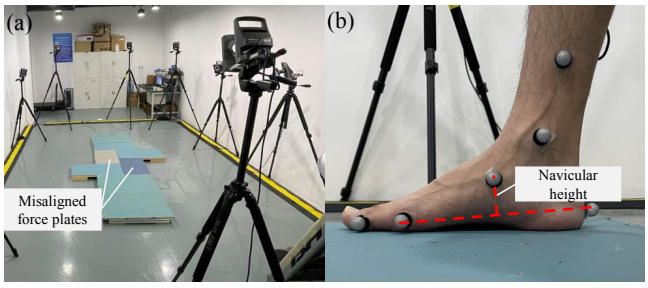

Fig. 2. (a) The layout of the experimental site with a 10-infrared camera motion capture system and two force plates. (b) The location of the 6 markers at one foot and the definition of arch height.

B. Quasi-Stiffness Estimation

Five young, healthy subjects (3 males and 2 females, age: 24 ± 2 years, height: 1.72 ± 0.05 m, mass: 65 ± 12 kg) gave their written consent and participated in the study. This study was approved by the Medical Ethics Committee of the School of Biomedical Engineering and Instrument Science, Zhejiang University (Project identification code: 2021-39).

Fig. 2(a) shows the layout of the human subject experimental site. All the subjects were told to walk on the 6-meter-long track at a comfortable pace and cadence for five repetitions. Foot kinematic data and GRFs were recorded to estimate changes in foot arch quasi-stiffness throughout the stance phase. Three-dimensional motion data were captured at 100 Hz using a 10-infrared camera motion capture system, whereas the GRF were collected synchronously at 1000 Hz using two 6-dimension force plates. The force plates were placed in a misaligned position to ensure that a complete stance phase of each foot was measured. As shown in Fig. 2(b), a total of 12 retro-reflective markers were attached to landmarks on both feet of each participant as described in [21].

All kinematic and GRF data were filtered offline using 8-point smoothing filters. The foot arch height was defined as the navicular height; see Fig. 2(b). The stance phase (from heel contact to toe-off) was defined with a 30 N vertical GRF threshold. The heel contact phase, plantar contact phase, and push-off phase were distinguished by the height of the posterior aspect of the calcaneus and first metatarsal head with a 20 mm height threshold. All kinematic and kinetic data were synchronized, and time normalized to stance phase duration.

Fig. 3(a) shows an example of the load on the foot arch versus the downward displacement of the foot arch of one subject. Additionally, in Fig. 3(b), arch quasi-stiffness exhibits notable dynamics: starting high in heel contact, it decreases, reaching a negative value in mid-plantar contact. In the push-off stage, arch quasi-stiffness sharply rises, peaking at a breakpoint (due to the change in the displacement direction). Subsequently, as the gait advances, foot arch stiffness gradually diminishes until lift-off. A negative arch quasi-stiffness implies that the foot was in a highly compliant state, that the foot adapted to the ground contact and absorbed

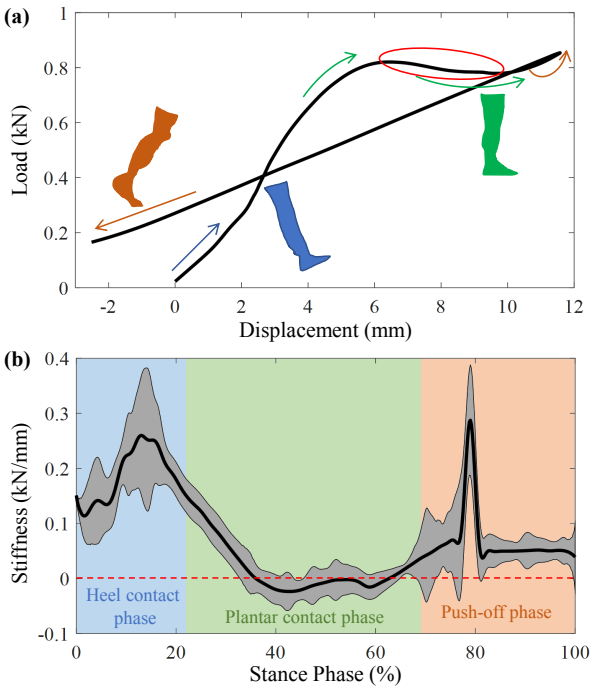

Fig. 3. (a) The load on the foot arch versus the downward displacement of the foot arch of a subject. (b) The variation of the foot arch's quasi-stiffness across the stance phase (mean of five subjects and standard deviation).

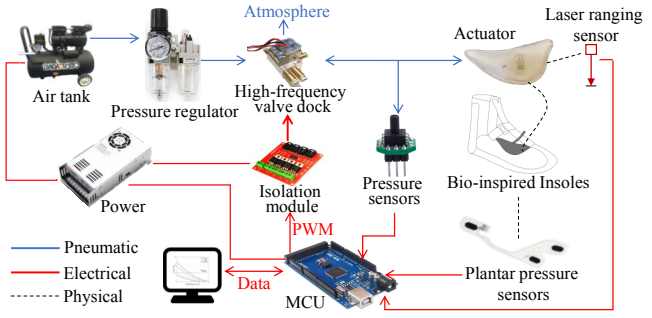

Fig. 4. Schematic of the the PASI and interconnection among sensors, actuators and embedded systems.

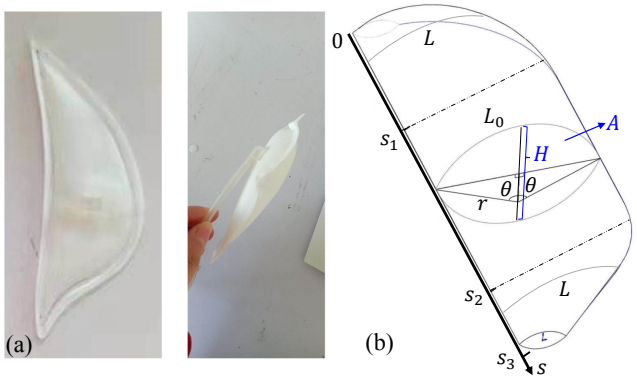

Fig. 5. (a) Actuator in inflated state and (b) physical model of the actuator.

energy by reducing the arch of the foot. Notably, although the results in [22] also indicate the negative quasi-stiffness in the plantar contact phase, this research is the first to report the continuous stiffness of the foot arch. It exclusively serves the control design for the following soft robotic device.

III. PASI Design and Foot-Insole Model

Fig. 4 illustrates the schematic of the pneumatic arch support insoles with embedded systems. The main components were two flexible bionic actuators attached to the insole and placed underneath the foot arch. The shape and structure of the actuator were intended to imitate the physiological shape of the regular foot's medial longitudinal arch for a better fit with the human foot arch. The PASI sensing suite also included plantar pressure sensors that measure the GRF and the gait phase, air pressure sensors to obtain the PSA pressure, and laser ranging sensors attached inside the PSA to measure the distance to the ground. A microprocessor, a power module, a set of high-speed solenoid valves, and an air tank are also included in the PASI.

A. Modeling of the Pneumatic Actuators

The PSA insole was manufactured through lamination and heat-sealing processes using a double layer of 40D nylon fabric with thermoplastic polyurethane. Fig 5 shows the prototype of the PSA and the modeling schematic. To build a physical model for the PSA, we consider the following assumptions: (1) The actuator undergoes a deformation process from a flat rectangular shape to a wing-shaped form. (2) There are no elastic energy losses during the deformation process. (3) The lengths in other directions of the actuator remain constant during the deformation process, with expansion and contraction occurring only in the vertical direction.

In order to obtain the PSA output, using the principle of virtual work and energy conservation, we describe the equilibrium between output work and input work as follows:

$$FdH = PdV, \tag{2}$$

where F is the output force of the actuator, P is the applied air pressure, and H and V are the height and volume of the actuator, respectively. Using the expansion geometry, we obtain

$$H(\theta) = \frac{L_0(1-\cos\theta)}{\theta},\ A(\theta) = \frac{L^2(\theta-\sin\theta\cos\theta)}{2\theta^2}. \tag{3}$$

where L_0 represents the middle curve length of the actuator surface, θ is the central angle of the actuator's expansion surface, A is the cross-sectional area during the actuator's expansion process, and L is the curve length of any cross-sectional area. Since the boundary of the actuator is an irregular curve, we approximate it by a set of arcs, straight lines, and diagonals (e.g., segments s_1, s_2, and s_3 in the figure). The internal gas volume V is then expressed as

$$V(\theta) = \int_\Gamma A(\theta)ds = \frac{(\theta-\sin\theta\cos\theta)}{2\theta^2}\int_\Gamma L^2(s)ds, \tag{4}$$

where Γ represents the boundary curve. From the above

calculation, we obtain

$$F = P\frac{dV/d\theta}{dH/d\theta} = P\Delta L\frac{\cos\theta(\sin\theta - \theta\cos\theta)}{\theta(\theta\sin\theta + \cos\theta - 1)} =: f(P,H), \tag{5}$$

where $\Delta L = \int_\Gamma L^2(s)ds/L_0$ is a geometric constant that can be obtained through the PSA design model. From (5), we express F as a function of P and H.

B. Physical Foot-Insole Interaction Model

Fig. 6 illustrates the foot-insole interactions. We model the foot-insole interactions as a mass-spring system, as shown in Fig. 6(b). The foot arch is considered as a point mass M and interacts with the ground through the spring with stiffness K. The height of the PSA actuator from the ground is denoted by x, and the body weight F_{GR} is applied at the top of the foot arch.

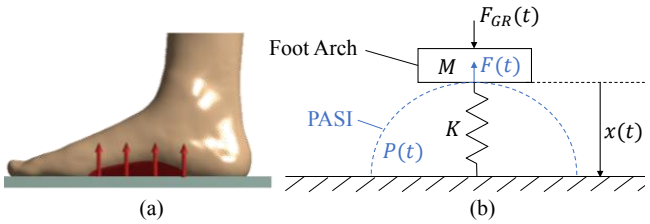

Fig. 6. (a) Schematic of PASI supporting the arch of the foot. (b) Mass–spring model of the foot-insole interaction dynamics.

The equation of motion of the foot-insole interaction is then given by

$$M\ddot{x}(t) + Kx(t) = F_{GR}(t) - F(t), \tag{6}$$

where $F(t) = f(P(t), x(t))$ is the PSA output force given by (5). Defining the discrete-time state variable $\boldsymbol{x}(k) = [x(k)\ \dot{x}(k)]^T$, $k \in \mathbb{N}$, we rewrite (6) as

$$\begin{aligned} x(k+1) &= x(k) + T_s\dot{x}(k), \\ \dot{x}(k+1) &= \dot{x}(k) - \tfrac{T_s}{M}[Kx(k) + f(u(k), x(k)) - F_{GR}], \end{aligned} \tag{7}$$

where $u = P$ is the control input and T_s is the sampling period. We further write the above dynamics and output into a compact form as

$$\begin{aligned} \boldsymbol{x}(k+1) &= \boldsymbol{f}_d(\boldsymbol{x}(k), u(k)) \\ \boldsymbol{y}(k) &= \boldsymbol{h}_d(\boldsymbol{x}(k), u(k)) \end{aligned} \tag{8}$$

where output $\boldsymbol{y}(k) = [x(k)\ F(k)]^T$ is obtained from sensor measurments and (5). Note that nonlinear functions $\boldsymbol{f}_d$ and $\boldsymbol{h}_d$ in (8) are from the dynamics and foot arch stiffness K is estimated by the method that was discussed in Section II.

IV. Dynamic Gait Support Control

A. Control Systems Overview

Fig. 7 shows the overview design of the dynamic plantar support control. A high-level pressure target generator and a low-level pressure controller are designed for the PASI. The high-level pressure target generator consists of a gait detection algorithm, the arch quasi-stiffness variation model presented in Section II, a PASI actuator model, the dynamics

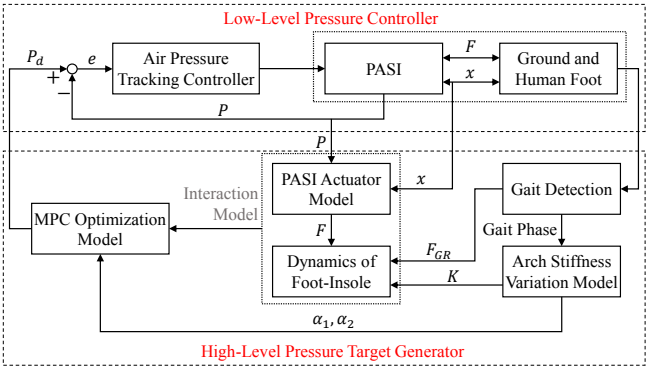

Fig. 7. Schematic of the control systems overview.

of foot-insole interaction, and an MPC scheme. The air pressure tracking controller is adopted to ensure the pressure of PASI tracks the desired profile. We discuss each part of the control design in this section.

B. MPC Design for Support Control

In this study, both assistive force $F(t)$ and the variation in foot arch height $x(t)$ are considered as design variables. Both of them are adjusted by the pressure P. Using the state-space model (8), we consider the output predictive and control horizon both as H, $H \in \mathbb{N}$ and the control input set $U_k = \{u(k), u(k+1), \cdots, u(k+H-1)\}$. The desired output at kth step is denoted as $\boldsymbol{y}_d(k) = [x_d(k)\ F_d(k)]^T$, where $x_d(t)$ and $F_d(t)$ are the desired profiles for displacement $x(t)$ and force $F(t)$.

The MPC is formulated as

$$\min_{U_k}\ J_k = \sum_{i=1}^{p} \boldsymbol{e}_y^T(k+i)\boldsymbol{W}\boldsymbol{e}_y(k+i) \tag{9a}$$

$$\text{subj. to: } x(k+i) = \boldsymbol{f}_d(\boldsymbol{x}(k+i), u(k+i)),$$

$$\boldsymbol{y}(k+i) = \boldsymbol{h}_d(\boldsymbol{x}(k+i), u(k+i)), \tag{9b}$$

$$\underline{u} \le u(k+i) \le \overline{u}, \tag{9c}$$

$$\underline{\Delta u} \le \Delta u(k+i) \le \overline{\Delta u},\ \ i = 1, \cdots, H, \tag{9d}$$

where output error $\boldsymbol{e}_y(k) = \boldsymbol{y}(k) - \boldsymbol{y}_d(k)$, $\boldsymbol{W} = \mathrm{diag}(\alpha_1/x_{\max}^2, \alpha_2/F_{\max}^2)$ is the weight matrix, $\alpha_1, \alpha_2 > 0$ are designed weights that will be discussed in the next subsection, and $x_{\max} = \sup_{t\ge 0} x(t)$ and $F_{\max} = \sup_{t\ge 0} F(t)$ are the upper bounds of $x(t)$ and $F(t)$, respectively. In constraint (9c), $\underline{u}$ and $\overline{u}$ are the lower and upper bounds of the input, respectively. For constraint (9d), $\Delta u(k) = u(k+1) - u(k)$, $\underline{\Delta u}$ and $\overline{\Delta u}$ are the lower and upper bounds of the input change rate, respectively. We solve the optimization problem (9) by using sequential quadratic programming algorithm at the kth time step. The first component of the solution U_k is applied to the system.

C. Gait-Adaptive Optimization

We propose a gait-adaptive optimization strategy for dynamic arch support during the stance phase. When specifying the desired output x_d and F_d, the PASI system should not

interfere with the natural deformation of the foot arch, while sufficient assistance is needed at the same time. In this study, x_d is each subject's normal variation measurement in arch height from Section II. F_d is derived from our companion study [23], which is about 15% of the GRF. With these considerations, we propose the weight adaptation and adjustment at various gait phases as follows:

$$\alpha_1 = \begin{cases} \sin\left(\frac{\pi}{2}\frac{t-t_h}{t_p-t_h}\right) & t_h \le t < t_p, \\ 1 & t_p \le t < t_o, \\ 0 & t_o \le t < t_h^*, \end{cases} \tag{10a}$$

$$\alpha_2 = \begin{cases} 1-\alpha_1 & t_h \le t < t_s, \\ 0 & t_s \le t < t_h^*, \end{cases} \tag{10b}$$

where $t \in [0, T_g]$ is the time in one gait cycle, T_g is the one gait duration, and t_h, t_p, t_o, t_s represent the time moment of heel-contact, plantar-contact, push-off, and swing phase events, respectively, and t_h^* represents the heel-contact timing in the next gait cycle.

When the foot arch is compressed and has negative quasi-stiffness during the plantar contact phase, the corresponding actuator needs to be compliant to not interfere with the compression and energy absorption of the foot arch. Therefore, the control target is to follow the foot arch's normal displacement, even providing insufficient support. When the foot arch becomes stiff during push-off, the actuator is inflated to provide support and additional stiffness for the foot arch to help release energy quickly. Hence, the control objective is to provide maximal assistance to facilitate the rapid elevation of the arch. Moreover, the arch stiffness transitions from high to low during the heel-contact phase. Hence, the weighting for displacement tracking follows the sinusoidal curve formula. During the swing phase, the arch is not under load, and the pressure in the actuator is maintained constant to prepare for the next heel contact.

D. Low-Level Control and Gait Detection

The PASI was connected to the air tank through a pressure regulator and 3/2 valves. The inflation speed of the PASI was controlled by regulating the duty cycle of the solenoid valve with a 90 Hz PWM signal generated from the MCU through an isolation power module. A closed-loop control system with a proportional-integral (PI) controller has been designed to quickly track the target air pressure. The control signals z can be obtained by the proportional module (P) and integral module (I) as follows:

$$\begin{aligned} \Delta z(k) &= k_p\left(e(k) - e(k-1)\right) + k_i e(k) \\ z(k) &= z(k-1) + \Delta z(k) \end{aligned} \tag{11}$$

where e ,k_p and k_i represent the error signal, proportionality coefficient, and integral coefficient, respectively.

Accurate GRF feedback from plantar pressure sensors and precise gait phase detection are crucial for implementing the PASI and the dynamic plantar support control. We rely on the algorithms from our previous studies [24], [25] to achieve real-time estimation of GRF. The heel contact phase, plantar contact phase, push-off phase, and swing phase are distinguished by the GRF of the forefoot and rearfoot measured by the plantar pressure sensors with a 10% body weight threshold. The accuracy of gait detection has been pre-calibrated through the motion capture system and force plates.

Algorithm 1 summarizes the overall execution of the gait detection and dynamic plantar support control.

Algorithm 1 Dynamic plantar support control

1: **Initialization**: Obtain the foot arch stiffness variation model and K, x_d, F_d
2: **repeat**
3: Gait detection and $x(k), P(k)$ measurement feedback
4: Calculate $F(k)$ using (5)
5: Predict $\{\boldsymbol{y}_d(k+1), \cdots, \boldsymbol{y}_d(k+H)\}$ using (8)
6: Calculate α_1 and α_2 by (10)
7: Solve the MPC (9) and obtain pressure control $u(k)$
8: Implement $u(k)$ by the PI controller
9: Execute foot arch support
10: **until** shut down the system

V. Experimental Results

A. Experiments and the PASI Testing

We first present the experiments for the force output characteristics of the PASI. Fig. 8(a) shows the load tester for the PASI. Under air pressures ranging from 40 to 200 kPa with an increment of 20 kPa, the vertical tensile force was recorded at 30 Hz as the load tester's upper portion moved downward at a constant speed (20 cm/min) from zero force until full compression or 15 mm displacement of the insole, with five repetitions. Fig. 8(b) shows the three-dimensional relationship between the PASI's force, displacement, and air pressure. The theoretical model then verified the force output measurements, with an average root mean square error of 12.5 N and 5.7% average relative error. Such model accuracy is sufficient for PASI-MPC implementation.

We then implemented and conducted the MPC-based dynamic plantar support control experiments. For the MPC implementation, we used the following parameters: $\underline{u} = 0$, $\overline{u} = 200$ kPa. $\underline{\Delta u} = -15$ kPa, $\overline{\Delta u} = 20$ kPa, $T_s = 5$ ms,

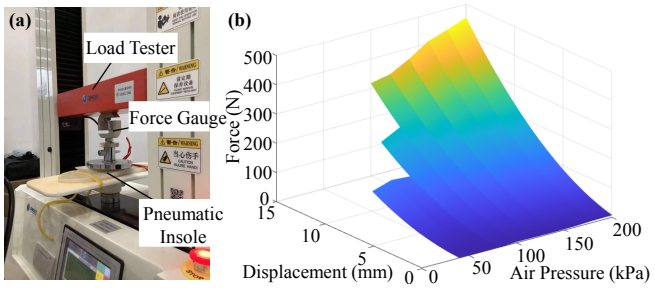

Fig. 8. (a) The load tester and the experiment setup of force output test. (b) The three-dimensional relationship between the force, displacement, and air pressure of the PASI.

$x_{\max} = 15$ mm, $F_{\max} = 1$ kN. We also selected the optimization threshold and PI control gains $k_p = 0.5$ and $k_i = 0.02$ for the PSA pressure control. The bandwidth of the pressure tracking controller is 2 Hz, and the rise time for a 100 kPa increment was around 0.18 s, as tested by the actuator's dynamic response tests.

B. Control Systems Performance

Subjects were instructed to traverse the terrain shown in Fig. 2 five times wearing the PASI system, during which the pressure, displacement, and force calculations were recorded. For comparison, a passive support mode was implemented, wherein the air pressure was maintained at 180 kPa. Additionally, the normalized root mean square tracking error (NRMSTE) of passive and MPC-based dynamic support were calculated in various gait phases (excluding the swing phase). The calculation of NRMSTE is given as

$$\text{NRMSTE} = \frac{1}{\max\|\boldsymbol{y}_d\| - \min\|\boldsymbol{y}_d\|}\sqrt{\frac{\sum_{i=1}^{n} \boldsymbol{e}_y^2(i)}{n}}, \quad (12)$$

where n is the sample number, $\max\|\boldsymbol{y}_d\|$ and $\min\|\boldsymbol{y}_d\|$ are the maximum and minimum values of norm of $\boldsymbol{y}_d$, respectively.

Fig. 9(a) illustrates the schematic of the gait phase detection, and Fig. 9(b) shows the target pressure profiles during the passive and dynamic supports (marked respectively as PS and DS). Figs. 9(c) and 9(d) show the displacement and force control results of a representative subject, respectively. Table I lists the NRMSTE values from these experiments. The results confirmed that the MPC-based dynamic support control achieved the desired objectives in each gait phase, particularly following the displacement during the plantar contact phase and providing assistance during the push-off phase.

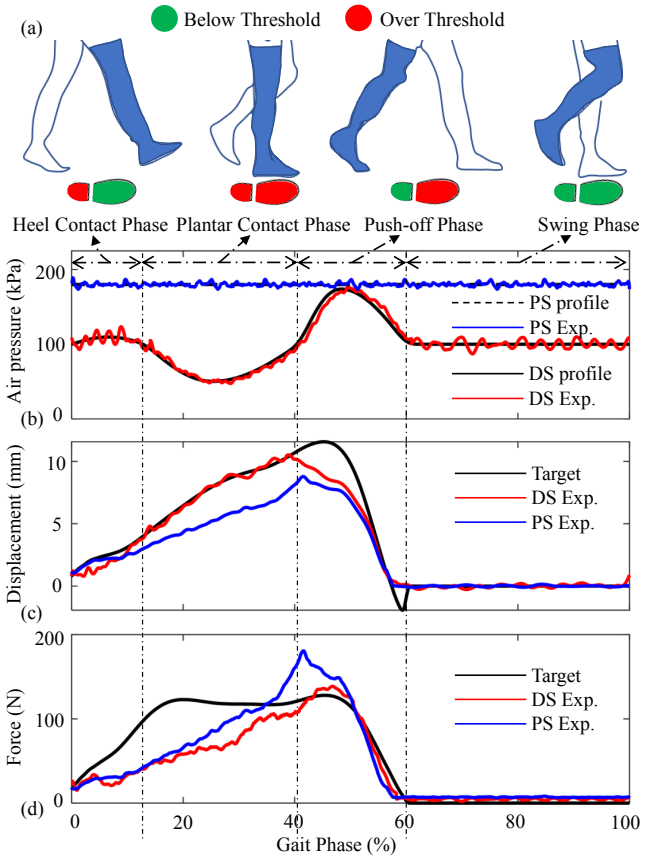

Fig. 9. (a) Gait phase detection. (b) The target pressure profile of the PASI and tracking results. (c) Target displacement and experiment data. (d) Target force and experiment data.

TABLE I
NRMSTE OF BOTH CONTROL METHOD IN DIFFERENT GAIT PHASES (%).

Control method		Heel contact	Plantar contact	Push-off
Displacement	MPC	5.2 ± 0.5	1.91 ± 0.2	16.5 ± 5.3
	Passive	4.77 ± 0.6	22.1 ± 6.6	23.1 ± 7.9
Force	MPC	27.8 ± 9.5	38.6 ± 12.8	7.14 ± 1.9
	Passive	26 ± 8.4	30.7 ± 8.1	23.0 ± 7.6

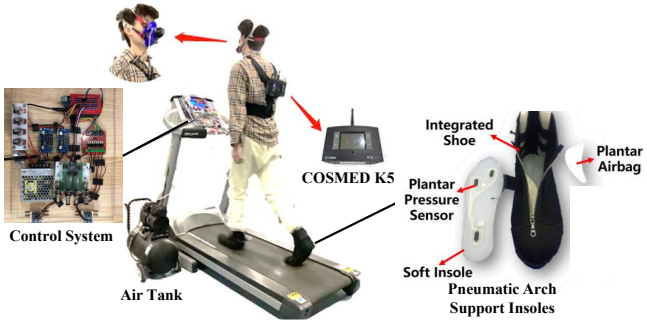

Fig. 10. The layout of 6-minute walking experiment.

C. Metabolic Walking Experiment

All five subjects continued participating in the metabolic walking test, as shown in Fig. 10. The metabolic equivalents (METs) were used to represent the metabolic cost by measuring the oxygen uptake (by gas analyzer K5 from COSMED, Italy) [26]. 1 MET is defined as 3.5 milliliters of oxygen per kilogram of body weight per minute, approximately equivalent to a person's oxygen consumption at rest with no activity [26]. An activity with an intensity of 5 METs signifies that the oxygen consumption during the activity is five times that of the resting state.

The subjects were first asked to wear the K5 device and the PASI with the power off to stand still for 6 mins, and the METs in the standing state were recorded. Afterward, the subjects were asked to walk on a treadmill at a constant speed (3.6 km/h) for 6 mins [27] wearing the PASI system. In order to address the effectiveness of the dynamic support control in reducing metabolic consumption, we designed three experimental conditions, including powered-off, dynamic support, and passive support condition (with a fixed 180 kPa pressure). The passive support condition represents the traditional rigid support insole or orthosis. The METs of subjects walking on the treadmill for 6 mins

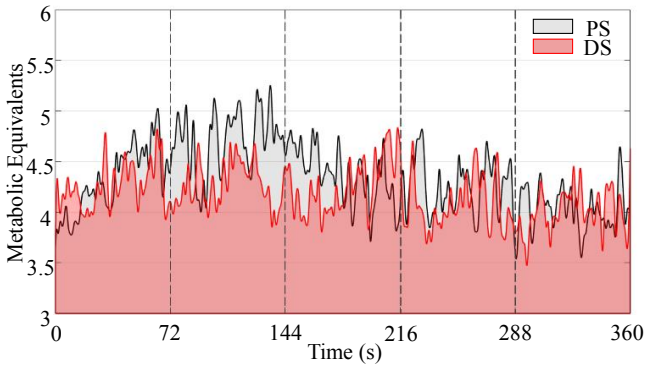

Fig. 11. METs of one subject in walking experiment with passive or dynamic support of the PASI.

TABLE II
METS OF EACH SUBJECT UNDER THREE CONDITIONS.

Subject	Powered-off	Dynamic support	Passive support
1	4.25	3.81	4.41
2	3.90	3.68	4.09
3	4.05	3.73	4.07
4	4.12	3.77	4.23
5	3.84	3.56	4.69
Mean	4.03	3.71	4.30
Stand. Dev.	0.17	0.10	0.26

under each experimental condition were recorded. Before the experiment, all subjects were given sufficient time to adapt to the system in each supporting condition. The order in which all the subjects experienced different experimental conditions was randomized.

We conducted paired two-sided t-tests to compare the dynamic and passive supports with the powered-off conditions and identify which condition exacted a significant change. Fig. 11 shows the METs of a participant during the 6-min walking experiment, comparing the passive support with the dynamic support condition. Overall, the METs in the dynamic support are lower than those in the passive support condition, indicating the effectiveness of the PASI and the MPC design during walking. Table II lists the average METs in 6-min walking under the three conditions for all subjects. The metabolic cost under the dynamic support was reduced by an average of 7.99% compared with the powered-off condition with a significant difference by two-sided t-test ($p = 0.0009$). On the contrary, the metabolic cost increased by an average of 6.60% under the passive support condition, but the two-sided t-test did not show a significant difference ($p = 0.15$).

VI. DISCUSSION AND CONCLUSION

This study is the first to propose the continuous variation of foot arch quasi-stiffness during walking and design a control strategy for dynamic, active assistance. Commencing with the integration of human-centric factors into the assistance paradigm, we presented a gait-adaptive model predictive control based on arch quasi-stiffness variation for a pneumatic plantar support insole. We first conducted the experimental estimation of the changing arch stiffness. The design of the PASI and MPC-based dynamic support control were then proposed and validated. Further, metabolic walking tests in five subjects were conducted. The results confirmed that adjusting the dynamic support of the arch according to its stiffness variation characteristics can reduce the metabolic cost of walking.

The implementation of PASI-MPC dynamic support control generated a reasonable pressure profile, which demonstrated better tracking of target displacement and assistance force than passive support. Notably, the NRMSTE for displacement tracking during plantar contact and force tracking during push-off were significantly lower than those for passive support (1.91% compared to 22.1% and 7.14% compared to 23%, respectively). The tracking performance during the heel contact phase was similar to that of passive support.

The PASI-MPC regulation on the foot arch that follows changes in the quasi-stiffness of the arch itself can reduce walking energy costs. The metabolic cost of walking was increased under the passive support condition, which agrees with the results in [11], except that the latter was proposed in the running condition. It can be attributed to the compression of the foot's plantar fascia, muscles, and tissues caused by the relatively rigid actuator, which hinders the energy absorption and release of the foot arch. It is representative of many conventional rigid orthotics that provide passive assistance [5]–[10]. However, with the PASI-MPC development, the foot was switched between flexibility and rigidity whenever needed without affecting the arch's ability to absorb energy in the plantar contact phase fully, and it provided the necessary stiffness during push-off. The metabolic cost of 5 subjects under the dynamic support condition was significantly smaller than that under the powered-off condition, with a maximum reduction of 10.4%.

This work provides inspiration and reference for designing and controlling foot orthotics and intelligent assistive devices for the lower limb. Foot assistive devices should have the ability of dynamic regulation to assist when the foot turns stiff and become flexible when the foot needs to absorb impact. This study also provides a reference value for human-machine interaction modeling and high-level control with pneumatic soft actuators, emphasizing the need to go beyond pressure or position tracking.

REFERENCES

[1] R. C. Aland and A. C. Sharp, "Anomalous plantar intrinsic foot muscle attaching to the medial longitudinal arch: possible mechanism for medial nerve entrapment: a case report," J. Med. Case Rep., vol. 15, no.1, 2021.

[2] J. Niu, Y. Zheng, H. Liu et al. "Stumbling Orediction Based on Plantar Pressure Distribution," Work, vol. 64, no. 1, pp. 1–8, 2019.

[3] J. M. Bukowska, M. Jekieek, D. Kruczkowski et al. "Biomechanical aspects of the foot arch, body balance and body weight composition of boys training football," Int. J. Environ. Res. Public Health, vol. 18, no. 9, pp. 5017–5029, 2021.

[4] D. Richie, "Biomechanics and Orthotic Treatment of the Adult Acquired Flatfoot," Clin. Podiatr. Med. Surg., vol. 37, no. 1, pp. 71–89, 2020.
[5] C. Neville, M. Bucklin, and N. Ordway, "An ankle foot orthosis with a lateral extension reduces forefoot abduction in subjects with stage II posterior tibial tendon dysfunction," J. Orthop. & Sports. Phys. Ther., vol. 46, no. 1, pp.1–26, 2016.
[6] I. Gómez-Jurado, J. M. Juárez-Jiménez, and P. Munuera-Martínez, "Orthotic treatment for stage I and II posterior tibial tendon dysfunction (flat foot): A systematic review," Clin. Rehabil., vol. 35 no. 2, pp. 159–168, 2021.
[7] S. Su, Z. Mo, J. Guo et al. "The effect of arch height and material hardness of personalized insole on correction and tissues of flatfoot," J. Healthc. Eng., vol. 2017, pp. 1–9, 2017.
[8] G. Desmyttere, M. Hajizadeh, J. Bleau et al. "Anti-pronator components are essential to effectively alter lower-limb kinematics and kinetics in individuals with flexible flatfeet," Clin. Biomech., vol. 86, no. 105390, 2021.
[9] Y. Jiang, D. Wang, J. Ying et al. "Design and preliminary validation of individual customized insole for adults with flexible flatfeet based on the plantar pressure redistribution," Sens., vol. 21, no. 5, pp. 1780, 2021.
[10] C. Neville, A. S. Flemister, and J. Houck, "Effects of the airLift PTTD brace on foot kinematics in subjects with stage II posterior tibial tendon dysfunction," J. Orthop. Sports. Phys. Ther., vol. 39, no. 3, pp. 201–209, 2009.
[11] S. M. Stearne, K. A. Mcdonald, J. A. Alderson et al. "The foot's arch and the energetics of human locomotion," Sci. Rep., vol. 6, pp. 19403, 2016.
[12] J. F. Geboers, J. H. Tuijl, H. A. Seelen et al. "Effect of immobilization on ankle dorsiflextion strengthScand," J. Rehabil. Med., vol. 32, pp. 66–71, 2000.
[13] D. Rus and M. T. Tolley, "Design, fabrication and control of soft robots," Nature., vol. 521, no. 7553, pp. 467–475, 2015.
[14] B. K. Dinh et al. "Hierarchical cascade controller for assistance modulation in a soft wearable arm exoskeleton," IEEE Robot. Autom. Lett., vol. 2, no. 3, pp. 1786–1793, 2017.
[15] C. Zhang, P. Zhu, Y. Lin et al., "Fluid-driven artificial muscles: biodesign, manufacturing, sensing, control, and applications," Bio-des. Manuf., vol. 4, pp. 123–145, 2021.
[16] M. Xiloyannis et al. "Soft robotic suits: state of the art, core technologies, and open challenges," IEEE Trans. Robot., vol. 38, no. 3, pp. 1343–1362, 2022.
[17] R. F. Ker, M. B. Bennett, S. R. Bibby et al. "The spring in the arch of the human foot," Nature., vol. 325, pp. 147–149, 1987.
[18] L. Welte, L. A. Kelly, G. A. Lichtwark et al. "Influence of the windlass mechanism on arch-spring mechanics during dynamic foot arch deformation," J. R. Soc. Interface, vol. 15, pp. 20180270, 2018.
[19] M. Venkadesan, A. Yawar, C. M. Eng et al. "Stiffness of the Human Foot and Evolution of the Transverse Arch," Nature., vol. 579, pp. 97–100, 2020.
[20] J. R. Rebula and A. D. Kuo, "The cost of leg forces in bipedal locomotion: a simple optimization study," PLoS ONE, vol. 10, pp. e0117384, 2015.
[21] F. Sichting and E. Florian, "The rise of the longitudinal arch when sitting, standing, and walking: contributions of the windlass mechanism," PLoS ONE, vol. 16, pp. e0249965, April 2021.
[22] M. Kondo, I. Yoshitaka, and K. Nobuhiro, "Relationship between forward propulsion and foot motion during gait in healthy young adults," J. Biomech., vol. 121, pp. 110431, 2021.
[23] Y. J. Zhang, X. Long, J. Y. Du et al. "Effect of soft inflatable orthosis on the medial longitudinal arch in patients with flexible flatfoot deformity," Clin. Biomech., vol. 88, pp. 105418, Aug 2021.
[24] X. Liu, X. Zhang, B. Zhang, B. Zhou, Z. He and T. Liu, "An IMU-based ground reaction force estimation method and its application in walking balance assessment," IEEE Trans. Neural. Syst. Rehabil. Eng., vol. 32, pp. 223-232, 2024.
[25] L. Wang, Q. Li, J. Yi, J. Zhang and T. Liu, "Real-time human lower limbs motion estimation and feedback for potential applications in robotic gait aid and training," 2021 IEEE International Conference on Robotics and Automation, Xi'an, China, 2021, pp. 8465-8471.
[26] B. A. Franklin, J. Brinks, K. Berra et al. "Using metabolic equivalents in clinical practice," Am. J. Cardiol., vol. 121, pp. 382–387, 2017.
[27] P. Meyns, Y. L. Kerkum, M. A. Brehm et al. "Ankle foot orthoses in cerebral palsy: effects of ankle stiffness on trunk kinematics, gait stability and energy cost of walking," Eur. J. Paediatr. Neurol., vol. 26, pp. 68–74, 2020.